Surface scaling analysis of a frustrated spring-network model for surfactant-templated hydrogels

G. M. Buendía,[1,2,*] S. J. Mitchell,[1,†] and P. A. Rikvold[1,‡]

[1]*Center for Materials Research and Technology, School of Computational Science and Information Technology,
and Department of Physics, Florida State University, Tallahassee, Florida 32306-4350*
[2]*Department of Physics, Universidad Simón Bolívar, Caracas 1080, Venezuela*

We propose and study a statistical-mechanical model, inspired by recent atomic force microscopy studies of the surface structures of crosslinked polymer gels into which voids are introduced through templating by surfactant micelles [M. Chakrapani *et al.*, e-print cond-mat/0112255]. The gel is represented by a frustrated, triangular network of nodes connected by springs of random equilibrium lengths. The nodes represent crosslinkers, and the springs correspond to polymer chains. The boundaries are fixed at the bottom, free at the top, and periodic in the lateral direction. Voids are introduced by deleting a proportion of the nodes and their associated springs. The model is numerically relaxed to a representative local energy minimum, resulting in an inhomogeneous, "clumpy" bulk structure. The free top surface is defined at evenly spaced points in the lateral (x) direction by the height of the topmost spring, measured from the bottom layer, $h(x)$. Its scaling properties are studied by calculating the root-mean-square surface width and the generalized increment correlation functions $C_q(x) = \langle |h(x_0 + x) - h(x_0)|^q \rangle$. The surface is found to have a nontrivial scaling behavior on small length scales, with a crossover to scale-independent behavior on large scales. As the vacancy concentration approaches the site-percolation limit, both the crossover length and the saturation value of the surface width diverge in a manner that appears to be proportional to the bulk connectivity length. This suggests that a percolation transition in the bulk also drives a similar divergence observed in surfactant templated polyacrylamide gels at high surfactant concentrations.

I. INTRODUCTION

Crosslinked polymer hydrogels are completely interconnected polymer networks that combine high water content with high porosity, forming macroscopic molecules that have applications in many fields. Their wide range of pore sizes makes such gels ideal for separation of biological macromolecules by electrophoresis or chromatography [1]. The crosslinking process induces a reorganization of the polymer structure, resulting in inhomogeneities in the spatial density [2–6]. These inhomogeneities affect the surface configurations of the gels, but only in recent years have advances in atomic force microscopy (AFM) made possible the imaging of soft material surfaces in an aqueous environment [7]. The effects of the crosslinking density, temperature, pressure, and sample thickness on the surface topography have been studied by Suzuki *et al.* [7,8]. Their results indicate that the structural features of the surface on both the micrometer and nanometer scales depend on these factors. It has been suggested [7] that control of the characteristic length scale of the gel surface using external stimuli may have applications in a variety of fields, such as regulation of adsorption and release of specific molecules by the intermolecular forces between the surface and the molecule. Thus, gel surfaces provide a unique opportunity to explore the interplay between phenomena on the macroscopic and nanoscopic scales.

Templated polyacrylamide gels are formed by polymerizing acrylamide with a crosslinker in the presence of a surfactant. The surfactant molecules form monodisperse micelles of a size roughly comparable with the crosslinker separation, and the presence of these micelles alters the gel pore structure, enhancing the gel's separation properties [9]. In a recent work the surface morphology of templated polyacrylamide gels was extensively studied by AFM and scaling analysis of the resulting images [10]. This study indicates that the gel surfaces are self-affine on short length scales, with roughness (Hurst) exponents on the order of 0.8–1. In the absence of surfactant a crossover length, above which the surface is no longer self-affine, was estimated to be on the order of 300 nm, and the saturation value of the interface width was on the order of 1 nm. Both values increased dramatically with the introduction of surfactant.

Detailed kinetic lattice models of the polymerization of crosslinked polymer gels have previously been constructed [11]. However, they emphasize the kinetics of polymerization and are extremely computationally intensive. Inspired by the experiments reported in Ref. [10], the aim of the present work is rather to construct and study a simple continuum model that can reproduce some of the observed scaling characteristics of the templated gel surfaces at a more modest (but still substantial) computational cost by concentrating on the elastic structure of the gel. In doing so, we neglect other aspects of polymer physics, in particular the excluded-volume interactions that are important to accurately describe structure on short length scales. Some preliminary results were presented in Ref. [12].

The remainder of this paper is organized as follows. In Sec. II we introduce the model and detail some aspects of the numerical calculations. In Sec. III we recall some scaling

---

*Electronic address: buendia@usb.ve
†Electronic address: s.mitchell@tue.nl
‡Electronic address: rikvold@csit.fsu.edu

concepts associated with the analysis of surfaces. In Sec. IV we show the results of our calculations, in particular, the scaling properties of the surface width and increment correlation function along with their dependence on the size of the sample. We also comment on the relevance of our results for the interpretation of recent AFM experiments. Finally, in Sec. V we present our conclusions.

II. MODEL

The model consists of a two-dimensional network of nodes interconnected by massless springs. The nodes represent crosslinker molecules, and the connecting springs represent polymer chains. The network topology consists of a triangular lattice of nodes, each of which is connected by harmonic springs to its six nearest neighbors (except at the top and bottom surfaces, where each node has only four connections). The model has no excluded-volume interactions, which limits its ability to accurately describe structure on short length scales. A triangular lattice was chosen to ensure geometrical stability in two dimensions without introducing bond-angle constraints. The corresponding unrealistically high crosslinker functionality should not significantly influence our results. The network has periodic boundary conditions in the horizontal (x) direction, free boundary conditions at the top ($y>0$) layer, and the nodes in the bottom layer are fixed at $y=0$, corresponding to bonding to a rigid substrate. There are L_x nodes in the horizontal direction and L_y nodes in the vertical direction.

The total energy of the network is $E=\Sigma_i(1/2)k_i(l_i-l_{0i})^2$, where k_i, l_i, and l_{0i}, are the spring constant, the actual length, and the equilibrium length under zero external force of the ith spring, respectively. (All quantities in this paper are given in dimensionless units.) The equilibrium length of each spring is independent of the other springs and is randomly chosen with probability density function (PDF)

$$P(l_{0i})=2\gamma l_{0i}\exp(-\gamma l_{0i}^2), \tag{1}$$

where γ is proportional to the inverse of the average number of monomers between crosslinkers. This PDF corresponds to the case that the equilibrium distance between crosslinkers is proportional to the square root of an exponentially distributed number of monomers. It is consistent with the picture that crosslinkers are distributed randomly along the polymer chains, and that a spring of equilibrium length l_{0i} corresponds to a polymer of the same average end-to-end distance in the random-coil collapsed phase [13,14]. The average equilibrium length of a spring is $\langle l_{0i}\rangle=\sqrt{\pi/\gamma}/2$. In agreement with a mean-field spin-chain approximation for the elastic properties of a collapsed polymer chain [14], we require that the elastic constant of the ith spring should be inversely proportional to its equilibrium length, $k_i=l_{0i}^{-1}$ in our dimensionless units.

With the above distribution of equilibrium lengths, the PDF for the force F exerted by a spring of length l is

$$P(F|l)=\frac{2\gamma l^2}{(1-F)^3}\exp\left[-\gamma\left(\frac{l}{1-F}\right)^2\right] \tag{2}$$

for $F\leq1$, while it vanishes for $F>1$. The average force exerted by a spring of length l is then

$$\langle F|l\rangle=1-l\sqrt{\gamma\pi}. \tag{3}$$

Initially, springs with equilibrium lengths drawn independently according to $P(l_0)$ are placed on the bonds of a regular triangular lattice of unit lattice constant, such that all of them are stretched or compressed to a length of one. In order that this initial configuration should not be globally stressed, we impose the condition that the average force exerted by a spring of unit length should be zero. By Eq. (3), this is satisfied for $\gamma=1/\pi$. However, the initial configuration is *locally* stressed, since $l_i=1$ for all i while $\langle l_{0i}\rangle=\pi/2\approx1.57$. The system is frustrated in the sense that there is no configuration that can simultaneously minimize the energies of all the springs. As a result there is a large number of configurations corresponding to local energy minima with similar energies.

The network was relaxed using the limited-memory Broyden-Fletcher-Goldfarb-Shanno (L-BFGS) quasi-Newton minimization algorithm [15,16] until a locally stable configuration was reached, corresponding to a local minimum in the global energy landscape. By minimizing several statistically equivalent realizations of the random spring configuration, we checked that the local minima reached by this procedure are representative of typical relaxed configurations. Although the total energies of different relaxed configurations were not completely identical, all the structural results were the same to within our numerical accuracy.

The L-BFGS subroutine requires the calculation of the total energy and its gradients, i.e., the local forces in the vertical and horizontal directions for each node. By monitoring the total energy and the absolute value of the force we found that the subroutine must be called about 3×10^4 times to ensure that the system reaches a local minimum. Since each relaxation step requires a new evaluation of the total energy and the local forces, the L-BFGS algorithm is quite computationally intensive, taking about 1–2 days on a current 600 MHz dual-processor Pentium III PC with 512 MB of shared memory to relax a typical system with about 10^6 degrees of freedom. However, it was far more efficient for our application than a naïve steepest-descent method, requiring about an order of magnitude less computer time while leading to essentially equivalent final energies and structures. After relaxation, we examined the bulk and surface properties of the network. Images of a typical relaxed network are shown in Figs. 1 and 2. Inhomogeneities in the spatial crosslinker density are evident in these figures.

III. SCALING PROPERTIES OF SURFACES

The scaling properties associated with the height fluctuations of rough surfaces have been the object of a great deal of interest. Vapor deposition, epitaxial growth, polymer growth, and many other phenomena exhibit scale invariance [17–20]. In a statistical sense, the height of a single-valued self-affine random surface, $h(x)$, satisfies the scaling relation
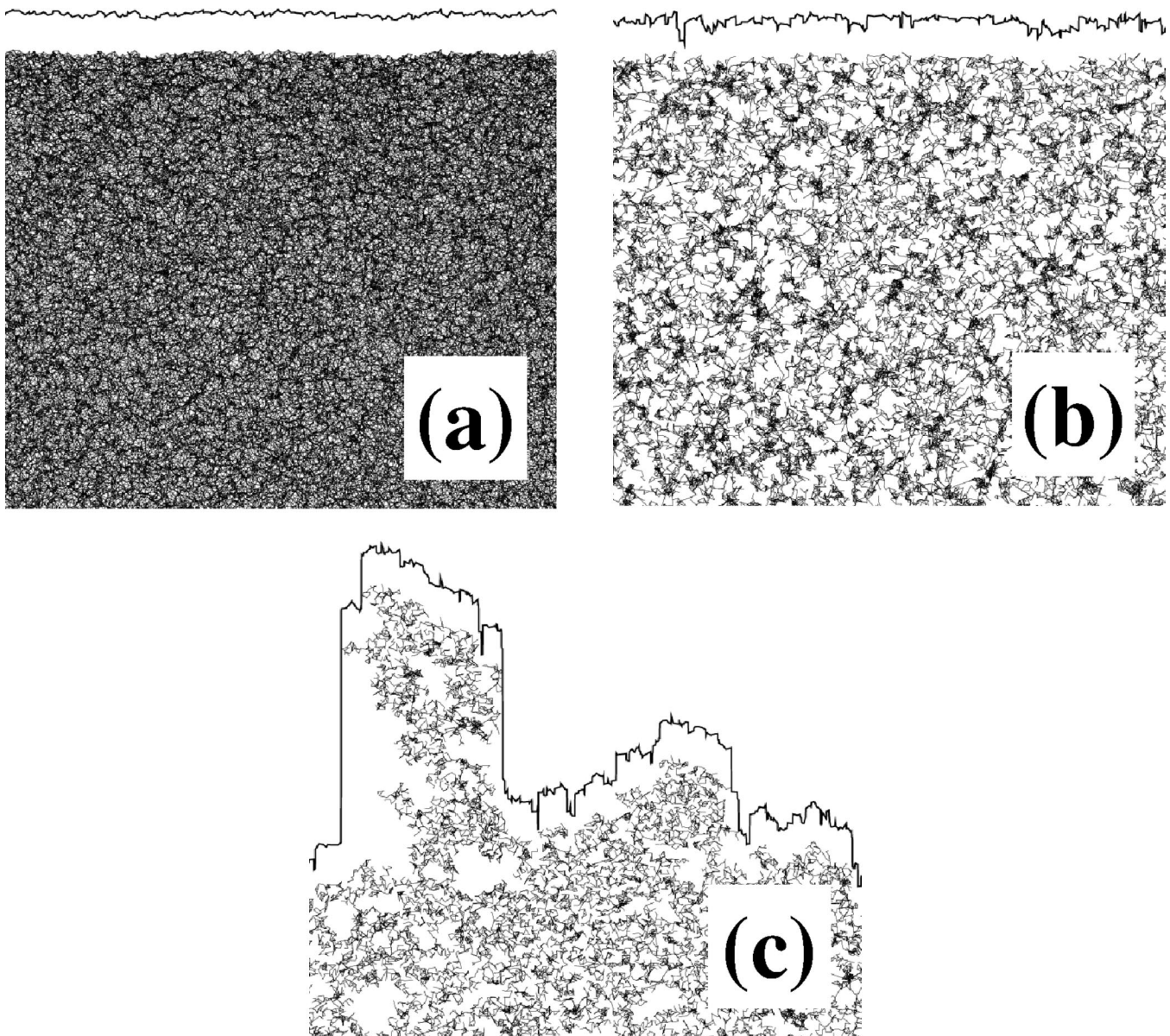
$$h(x)=\lambda^{-H}h(\lambda x), \tag{4}$$

FIG. 1. Details of the surface and bulk structures of relaxed 1024×768 systems with vacancy concentrations of (a) 0%, (b) 40%, and (c) 49.5%. The thin line segments represent polymer chains. The bold lines (vertically displaced for easier viewing) represent the free surface.

where λ is a dimensionless scaling parameter and H is the so-called Hurst exponent, which in this case is identical to the roughness exponent [20]. Consequently, the increment correlation function $C(x)$ of a translationally invariant, self-affine surface scales as

$$C(x) = \langle [h(x_0+x) - h(x_0)]^2 \rangle \sim x^{2H}, \qquad (5)$$

where the average is taken over x_0. Many surfaces present a mixed behavior characterized by

$$C(x) \sim \begin{cases} x^{2H} & \text{for } x \ll l_\times \\ \text{const} & \text{for } x \gg l_\times, \end{cases} \qquad (6)$$

where $l_\times$ is a crossover length scale separating the two behaviors. However, there exist surfaces for which the scaling cannot be described by a single exponent; instead an infinite hierarchy of characteristic exponents has to be introduced. These surfaces are called multiaffine, and they are occasionally observed in nature [21–23]. Molecular-beam epitaxy (MBE) models [24], polished metal surfaces [25], geomorphological features [26], and time series of financial data [27,28] provide some examples of multiaffine scaling. The characteristic exponents of a multiaffine function can be calculated from the qth order increment correlation function, defined as

$$C_q(x) = \langle |h(x_0+x) - h(x_0)|^q \rangle \sim x^{qH_q} \qquad (7)$$

with the generalized Hurst exponent H_q depending continuously on q, at least in some region of q values. Thus $C_2(x)$ is identical to the usual increment correlation function $C(x)$
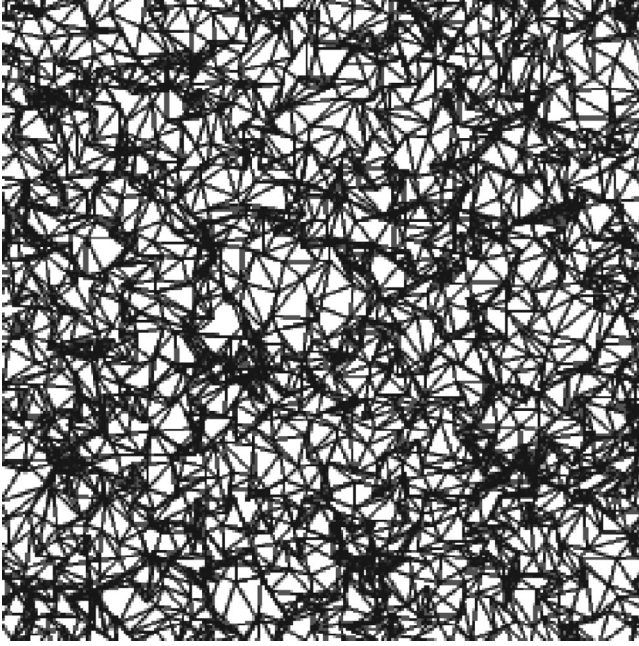
FIG. 2. Magnified detail of the relaxed bulk structure for a 1024×768 system without vacancies.

defined in Eq. (5). Like self-affine surfaces, multiaffine surfaces can show a crossover to scale-independent behavior, analogous to Eq. (6).

In the following section we present our results on the structure of the bulk and the scaling behavior of the surface, calculated after the spring network has been relaxed to a representative local energy minimum.

IV. NUMERICAL RESULTS

We analyzed spring networks of sizes $L_x \times L_y$. In order to simulate experimental measurements of the scaling behavior of surfaces of gels in which pores have been introduced by polymerizing acrylamide plus a crosslinker templated with surfactants that are later removed [9,10], we created voids in the networks. The voids were introduced by selecting a proportion of the nodes at random and removing these nodes and the springs associated with them. Next, the Hoshen-Kopelman algorithm [29,30] was applied to identify and discard clusters that were not connected to the fixed substrate. This last step is particularly important near the site-percolation limit, which for the triangular lattice is at a vacancy concentration of 50% [30,31]. Note that by ''vacancy concentration'' we always mean the initial concentration of vacant nodes before removal of the disconnected clusters. The total volume fraction of the void structure resulting from the cluster removal is of course larger.

We define the one-dimensional surface as the set of surface heights, $h(x_j)$, at equally spaced discrete points, $x_j \in [0, L_x]$, considering the polymer chains as straight line segments between nearest-neighbor connected nodes. To calculate the surface height at x_j, we first identify the set of all springs which intersect a vertical line at x_j. From this set of springs, we define

$$h(x_j) = \max[y_i(x_j)], \qquad (8)$$

where $y_i(x_j)$ is the vertical location of the intersection of the ith spring at x_j. We use the sign convention that $y = 0$ for the fixed bottom nodes and the free surface is located at positive values of y. In Fig. 1 we show details of the bulk and free surface of systems with vacancy concentrations of 0%, 40%, and 49.5%, while in Fig. 2 we show a magnified view of a section of the bulk of a vacancy-free system.

To obtain an estimate of the finite-size effects and select an appropriate system size for the production runs, we first considered vacancy-free spring networks of sizes $L_x \times L_y$, with $L_x = 512$, 1024, and 2048, and $L_y = 256$, 384, 512, 640, and 748. We calculated the root-mean-square width of the surface (also known as the rms roughness) on a length scale L, w_L, by recursively subdividing the surface into n non-overlapping segments of length $L = L_x/n$, with n an integer between 2 and $L_x/2$. The mean-square width of the kth segment is

$$w_{Lk}^2 = \langle y^2 \rangle_{Lk} - \langle y \rangle_{Lk}^2, \qquad (9)$$

where $\langle \ \rangle_{Lk}$ denotes averaging within the segment. The rms width is defined as the square root of the average of w_{Lk}^2 over the n segments, $w_L = \sqrt{n^{-1} \Sigma_{k=1}^n w_{Lk}^2}$. The statistical errors in w_L were estimated in the usual way from the standard deviation of w_{Lk}^2.

At this point we emphasize that the order in which the average and the square root are taken in the definition of w_L is important. For a simple self-affine surface it is irrelevant whether the square root is taken before or after the average; in either case one obtains the same exponent. However, for a multiaffine surface the results are quite different. In this case the exponent obtained from w_L is equal to that calculated from the increment correlation function $C(L)$ only when the average is calculated *before* taking the square root, as it is done here. The results for w_L, averaged over four independent configurations for each system size, are shown in Fig. 3.

The data shown in Fig. 3 indicate that, for the values of L_x and L_y considered, w_L is independent of the system size. However, when comparing the average height for the jth layer in the relaxed system, $\langle y_j \rangle$, with its original value in the regular triangular lattice, we found a slight contraction limited to approximately the top 250 layers. To minimize finite-size effects due to interference of the finite thickness L_y with this skin effect, while maintaining L_x as large as possible so as to reach large horizontal length scales and reduce statistical uncertainties in the estimates of w_L, we chose a system size of $L_x \times L_y = 1024 \times 768$ for the production runs. Both the bulk and surface structures were analyzed as discussed in the following two subsections.

A. Bulk structure

In this subsection, we discuss the bulk properties of the spring network far from both the fixed and free surfaces. We only present results for a gel without vacancies. For gels with high vacancy concentrations, it is difficult to define a bulk region, since the width of the surface region increases with
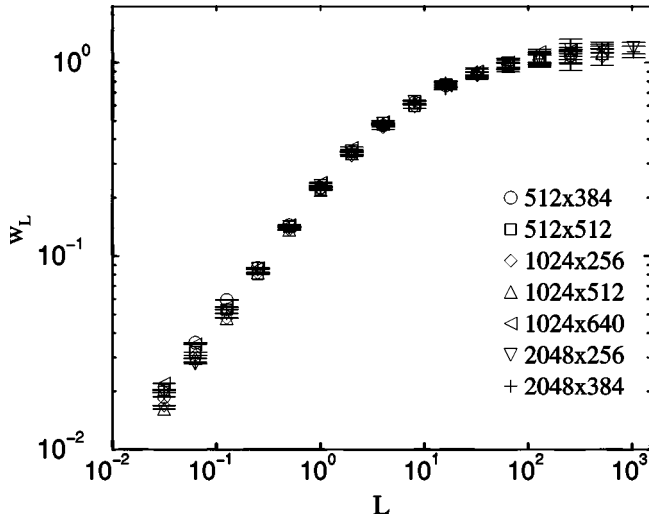
FIG. 3. The rms surface width w_L for vacancy-free spring networks, shown on a log-log scale as a function of the length scale L for a number of system sizes. The two scaling regimes defined in Eq. (6) are clearly seen. The data are averaged over four independent configurations for each system size.

FIG. 4. The bulk scale parameter vs the length scale L. The data are for a system of 1024×768 nodes with 0% vacancies, averaged over eight independent configurations. The function values near zero indicate randomly placed nodes at small length scales, and the maximum at $L \approx 1.57$, which is the average equilibrium spring length, indicates that nodes are most regularly placed on this scale.

increasing vacancy concentration. To study the bulk structure in this case, simulations with periodic boundary conditions would be preferable.

The presence of inhomogeneities in the spatial crosslinker distribution, where the crosslinkers and the polymer chains (shown as line segments) have greater densities in some regions (clumps), can be seen in Fig. 1 and Fig. 2. The effect is more pronounced for higher vacancy concentrations. This is a desirable feature of the model since static inhomogeneities are characteristic of crosslinked polyacrylamide gels and have been related to a freezing-in of the topological structure during polymerization [2–6]. For gels without vacancies, Fig. 1(a), the clumping is not as obvious to the eye. Thus, we show in Fig. 2 a magnified image of a small region of the bulk of a vacancy-free system, in which the clumping can be clearly seen. To quantify the clumping, we characterize the bulk scaling properties of the gel by a method analogous to the width-scaling method of Eq. (9).

We define $\rho(x,y) = \Sigma_i \delta(x - x_i, y - y_i)$ to be the density of nodes at a particular point (x,y) of the bulk. Here $\delta(\cdot)$ is the two-dimensional Dirac delta function, and the sum runs over all nodes (x_i, y_i) in the system. We calculate the mean and the variance of the number of nodes inside a box of side L, $\langle N \rangle_L$ and $\langle N^2 \rangle_L - \langle N \rangle_L^2$, respectively, by averaging $\rho(x,y)$ over nonoverlapping boxes. When there are no correlations within the gel, corresponding to a purely random distribution of node positions, the number of nodes in a box obeys a Poisson distribution. This yields $\langle N \rangle_L / (\langle N^2 \rangle_L - \langle N \rangle_L^2) = 1$. However, when the nodes have a more regular distribution, the denominator is reduced and the ratio increases. In Fig. 4 $\langle N \rangle_L / (\langle N^2 \rangle_L - \langle N \rangle_L^2) - 1$, averaged over eight independent realizations of the system, is shown vs L from $L = 0.25$ to 10. For small L, the function tends to zero, indicating that nodes that are very close together are essentially randomly placed. The function goes through a maximum near the average spring length ($L \approx 1.57$), corresponding to a more regular
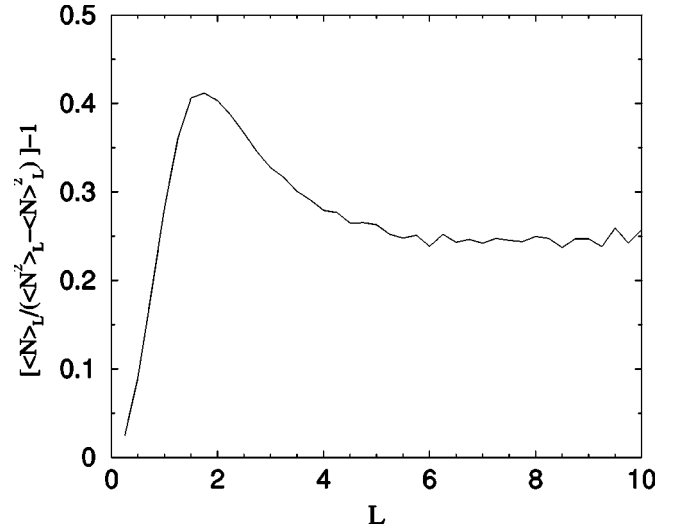
distribution of the nodes on this scale. Inclusion of excluded-volume interactions would modify the bulk correlations for small distances, relative to the present model.

B. Surface scaling behavior

We calculated the qth root of the qth order increment correlation function, $C_q^{1/q}(L)$, for $q = 0.5$, 1, 1.5, 2, and 2.5. The results for systems with 0%, 40%, and 49.5% vacancies are shown in Figs. 5(a), 5(b), and 5(c), respectively. For each of the two lower vacancy concentrations the data were averaged over ten independent realizations of the system, while thirteen realizations were used for the highest concentration. For all three vacancy concentrations, the surface is seen to be multiaffine with q-dependent slopes for L below a crossover length, $l_\times$. [For the highest vacancy concentration, Fig. 5(c), two scaling regimes with different, nonzero H_q are seen for $q \leq 1$.] For $L > l_\times$, $C_q^{1/q}$ reaches a saturation value $C_{\text{sat}}^{1/q}$. Both of these length scales, $l_\times$ and $C_{\text{sat}}^{1/q}$, depend on the vacancy concentration and q in ways that are discussed below.

By numerically calculating the logarithmic derivatives of the correlation functions with respect to L we determine the scaling exponents,

$$H_q = \frac{1}{q} \frac{d \log C_q(L)}{d \log L}. \tag{10}$$

Effective values for H_q for different L and q were estimated as two-point derivatives over intervals corresponding to a doubling of L. The results are shown in Figs. 6(a), 6(b), and 6(c) for systems with 0%, 40%, and 49.5% vacancies, respectively. The figures clearly indicate that on length scales below $l_\times$, the surfaces are multiaffine with q-dependent scaling exponents H_q. In this scaling regime the effective
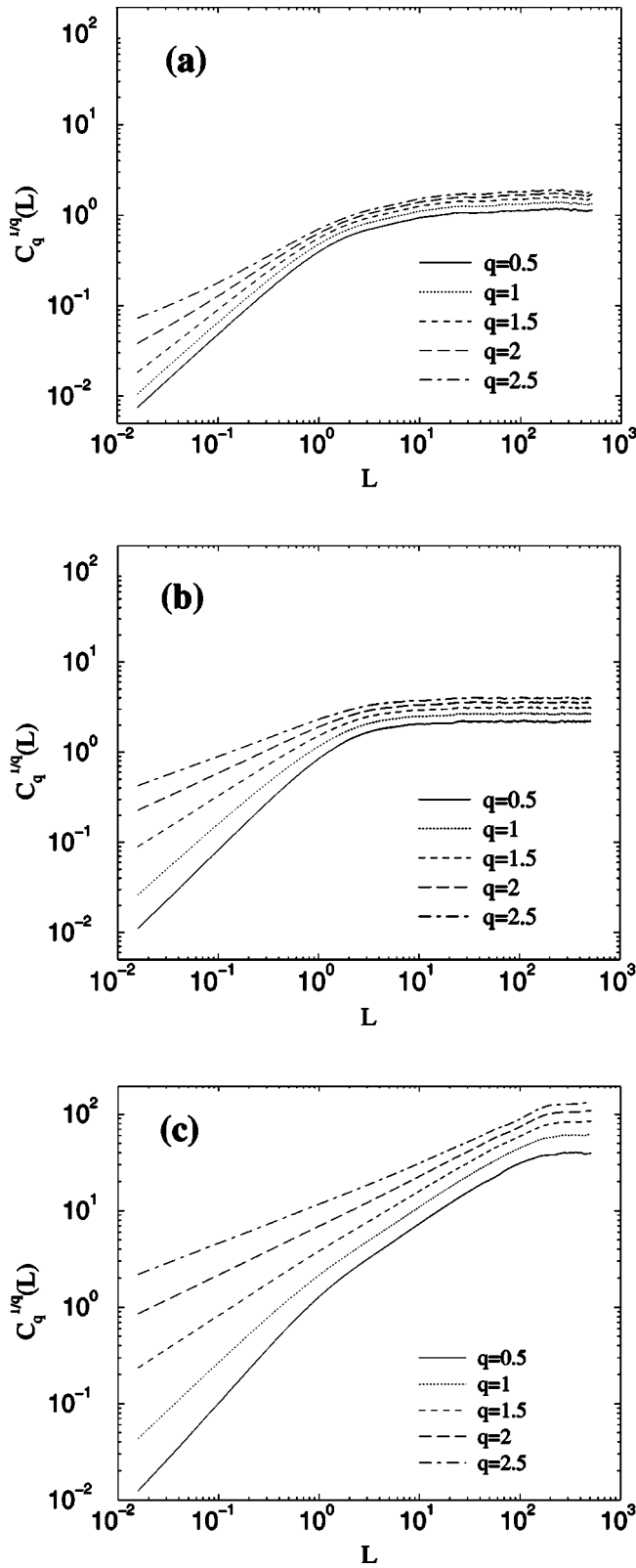
FIG. 5. The qth root of the generalized increment correlation function $C_q(L)$ for systems with vacancy concentrations (a) 0% vacancies, averaged over ten independent realizations. (b) 40% vacancies, averaged over ten independent realizations. (c) 49.5% vacancies, averaged over thirteen independent realizations.
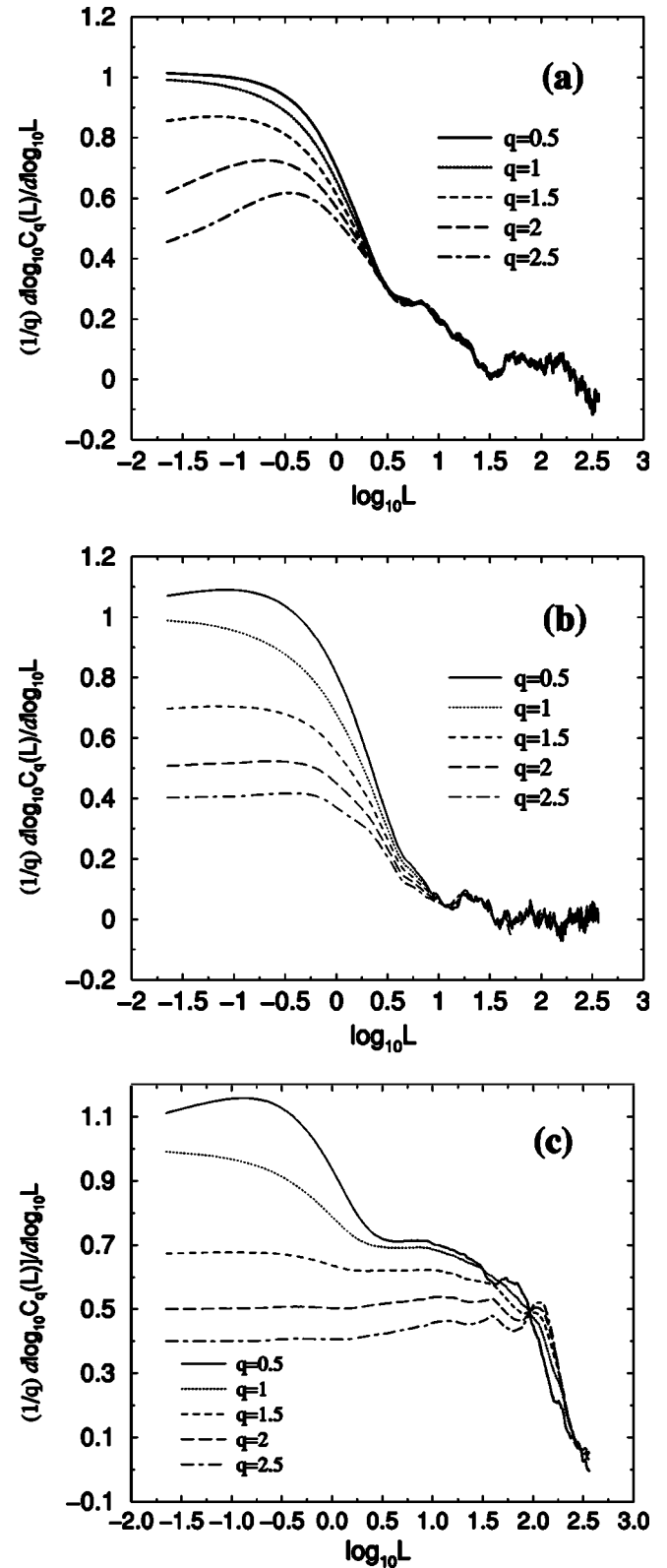
FIG. 6. The effective generalized Hurst exponent H_q for systems with different vacancy concentrations, obtained as logarithmic two-point derivatives of $C_q^{1/q}(L)$ with respect to L. The data for $C_q^{1/q}(L)$ were averaged as in Fig. 5. For small L and q, the derivative approaches unity, indicating $H_q \approx 1.0$. For large L, H_q approaches zero, signaling the scale-independent saturation regime. (a) 0% vacancies. (b) 40% vacancies. (c) 49.5% vacancies.

TABLE I. Scaling exponent H_q: dependence on q and vacancy concentration.

Vacancies (%)	$H_{0.5}$	H_1	$H_{1.5}$	H_2	$H_{2.5}$
0	1.0008	0.9682	0.8683	0.7030	0.5428
10	1.0113	0.9649	0.8232	0.6268	0.4688
20	1.0286	0.9543	0.7657	0.5627	0.42577
30	1.0541	0.9541	0.7212	0.5256	0.4088
40	1.0910	0.9607	0.7045	0.5168	0.4059
45	1.1087	0.9588	0.6940	0.5105	0.4019
47	1.158	0.9713	0.6939	0.5105	0.4019
49	1.140	0.9662	0.6820	0.5052	0.4021
49.5	1.1552	0.9711	0.6772	0.5025	0.4008

exponents are approximately independent of L. Scaling exponents H_q for different values of the vacancy concentration are presented in Table I. The exponents shown in this table were obtained from Eq. (10) at fixed $L=0.088$, in the small-L scaling regime. In Fig. 7 we show how these values of H_q change with q and the vacancy concentration. For $q>1$, H_q decreases with increasing vacancy concentration, while it increases for $q<1$. For $q=1$, H_q is slightly below unity and independent of the vacancy concentration to within our numerical accuracy.

Multiaffinity is relatively rare in natural surfaces, and, in fact, it is not observed in the experimental system that inspired the present study [10]. It is therefore reasonable to inquire about the source of the multiaffinity observed in our model. We find that it is caused by the finite density of discontinuities, which result from overhangs in the simulated surfaces (see Fig. 1). This effect is illustrated in two ways in Fig. 8. In Fig. 8(a) we show on a log-log scale $C_q(L)^{1/q}$ for different values of q for surfaces generated by fitting linear line segments of unit length to self-affine surfaces with a Hurst exponent of 0.75, which were generated by the method of successive additions [32]. These surfaces are seen to be self-affine with a Hurst exponent which crosses over from near unity to approximately 0.75 at about $L=1$. In the same figure we also show (by thin curves) the corresponding generalized increment correlation functions for surfaces generated from the above ones by the insertion of a finite density of vertical discontinuities. In contrast to the result for the original surfaces, the slopes of the latter curves depend on q, indicating that the discontinuous surfaces are multiaffine. Conversely, in Fig. 8(b) we illustrate the effect of removing the discontinuities from a surface generated by our model with 0% vacancies. While the original surface is multiaffine (signified by the q-dependent slopes), the surface from which the discontinuities are removed is self-affine with a Hurst exponent of approximately 0.98, corresponding to the straight line segments used to represent the polymer chains. These numerical results clearly show that the multiaffinity in our model surfaces is due to the vertical discontinuities caused by the overhangs. Possible methods to improve the agreement of the scaling behavior of the model surfaces with that of the experimental system by removing the discontinuities are discussed in Sec. V.

The large-L saturation values, $C_{\text{sat}}^{1/q}$, are summarized in
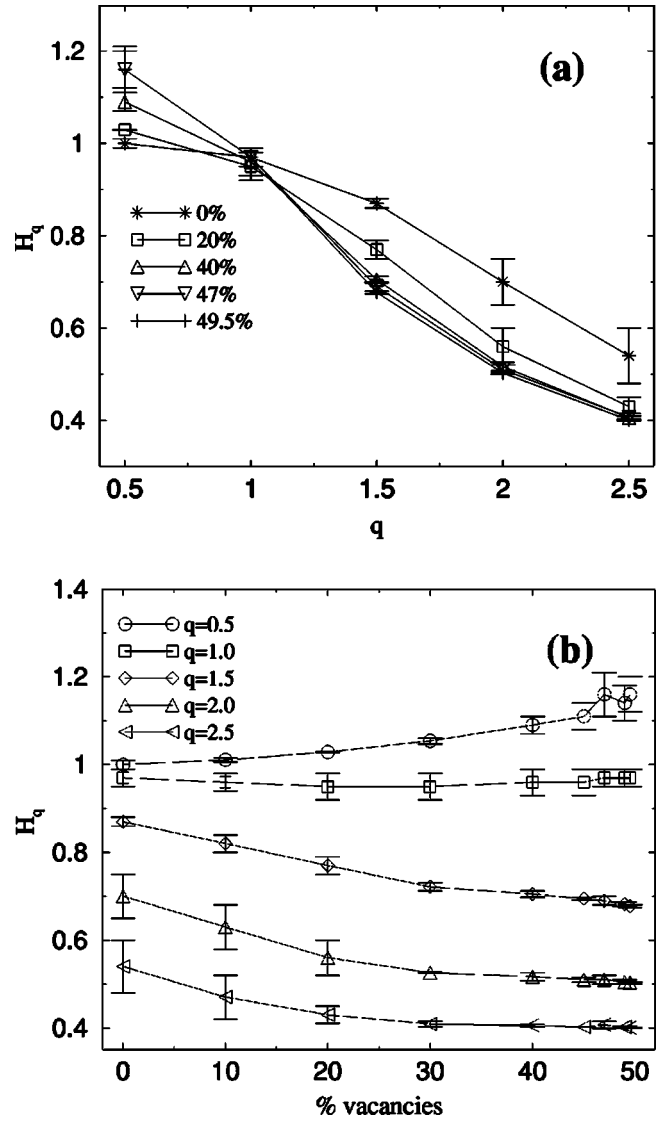

FIG. 7. The generalized Hurst exponent H_q for systems with different vacancy concentrations, from Table I. (a) Shown vs q for different vacancy concentrations. (b) Shown vs vacancy concentration for different values of q. In both parts the lines are merely guides to the eye.

Fig. 9. For a fixed concentration of vacancies, the saturation value increases with increasing q. The saturation value also increases with the vacancy concentration, quite dramatically so when the concentration approaches the site-percolation limit of 50%. Figure 9(a) shows $C_{\text{sat}}^{1/q}$ versus the vacancy concentration on a linear-log scale, while Fig. 9(b) shows the same quantity versus the relative distance from the percolation limit, $\epsilon=1-(\%\,\text{vacancies})/50\%$, on a log-log scale. The straight line in Fig. 9(b) is proportional to $\epsilon^{-\nu}$ with $\nu=4/3$ being the exact value for the connectivity-length exponent [30,31]. The figure indicates that $C_{\text{sat}}^{1/q}$ appears to be coupled to the connectivity length for vacancy percolation in the bulk, at least for $q\geqslant1$.

For a given vacancy concentration, all the curves in Fig. 6 coincide for $L\gtrsim l_\times$, indicating that the surface structure is not scale dependent on these large length scales. Due to the
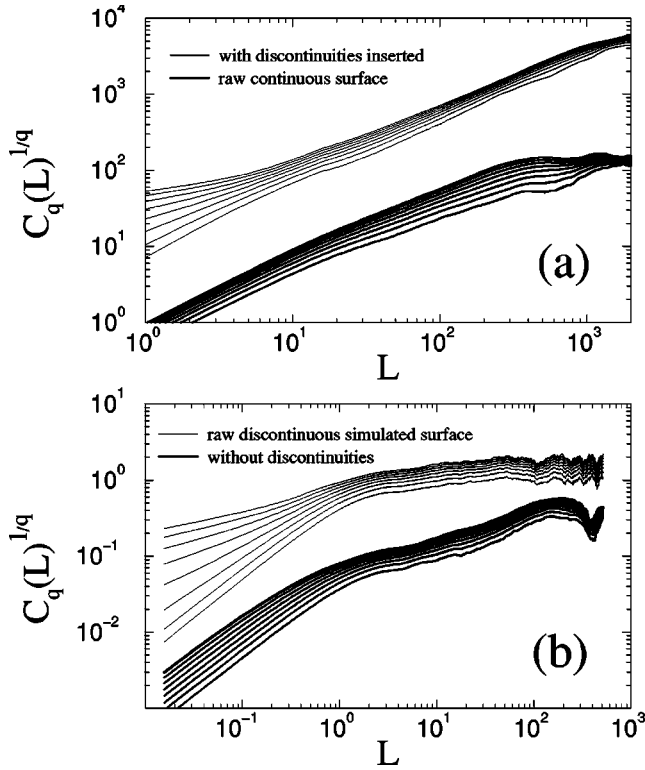
FIG. 8. Effects of discontinuities on the generalized correlation functions $C_q(L)^{1/q}$ and their logarithmic slopes, the generalized Hurst exponents H_q, for self-affine and multiaffine surfaces. In all sets of curves shown, q goes from 0.5 to 4.0 in increments of 0.5, from below to above in the figures. For clarity of view, the data corresponding to continuous surfaces (the thick curves) have been divided by ten. (a) The thick curves correspond to continuous, approximately self-affine surfaces, as indicated by the q-independent H_q. The thin curves represent discontinuous surfaces obtained by inserting a finite density of vertical discontinuities in the original surfaces. For the latter surfaces, H_q depends on q, indicating multiaffinity on length scales less than ten. Each curve is an average over data for 1000 surfaces. (b) The thin curves correspond to a multiaffine simulated gel surface with 0% vacancies, corresponding to those for which $C_q(L)^{1/q}$ are shown in Fig. 5(a). The thick curves correspond to a continuous surface generated from the simulated gel surface by removing all vertical discontinuities. In this case, H_q is independent of q, indicating simple self-affinity.

difficulty in obtaining a precise estimate for $l_\times$, we chose to define it as the value of L at which $H_q = 0.3$. This value is shown versus the vacancy concentration in Fig. 10 which, like Fig. 9, is divided into two parts. In Fig. 10(a) $l_\times$ is shown versus the vacancy concentration on a linear-log scale, while in Fig. 10(b) it is shown versus ϵ on a log-log scale. The increase in the vicinity of the percolation threshold is similar to that of $C_{\text{sat}}^{1/q}$ in Fig. 9, except that $l_\times$ has a significant background value that dominates at and below a vacancy concentration of 40% ($\epsilon \gtrsim 0.2$). Thus our data indicate that both these characteristic surface lengths are coupled to the bulk connectivity length as percolation is approached. Similar behavior to that observed for the saturation value of $C_2(L)^{1/2}$ is also seen for the saturation value of w_L.

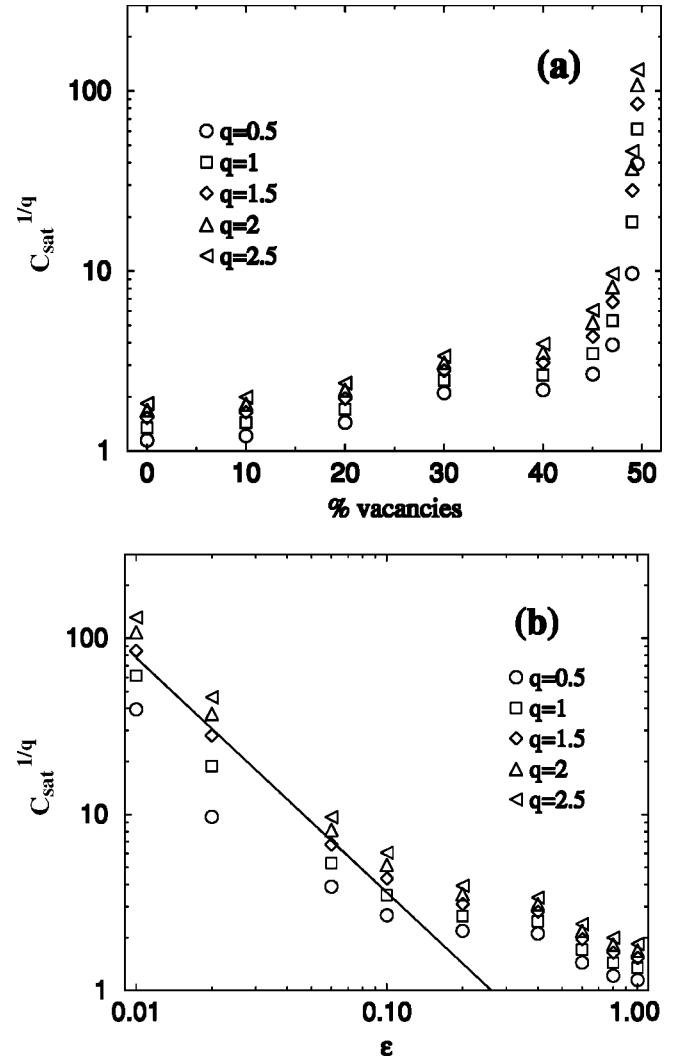In the templated polyacrylamide gels studied in Ref. [10],

FIG. 9. The large-L saturation value of $C_q^{1/q}(L)$, $C_{\text{sat}}^{1/q}$. (a) Shown vs vacancy concentration on a linear-log scale. (b) Shown vs $\epsilon = 1 - (\% \text{ vacancies})/50\%$ on a log-log scale. (Note that the vacancy concentration here increases toward the *left*.) The straight line is proportional to $\epsilon^{-4/3}$, corresponding to the connectivity length for bulk site percolation [30,31]. In both parts the error bars are smaller than the symbol size.

a strong increase in the crossover length and surface width at surfactant concentrations above 20% by weight coincides with a change from an optically clear material to a white, opaque one. Such a change in the light scattering intensity is consistent with an increase in the bulk correlation length from much smaller than, to on the order of the wavelength of visible light. Considering the numerical and experimental evidence together, we conclude that the dramatic increases in the surface-related length scales that occur with increasing volume fraction of voids are related to a percolation transition in the system of vacancies in the bulk, both in our model and in the experimental system by which it was inspired.

V. SUMMARY AND CONCLUSIONS

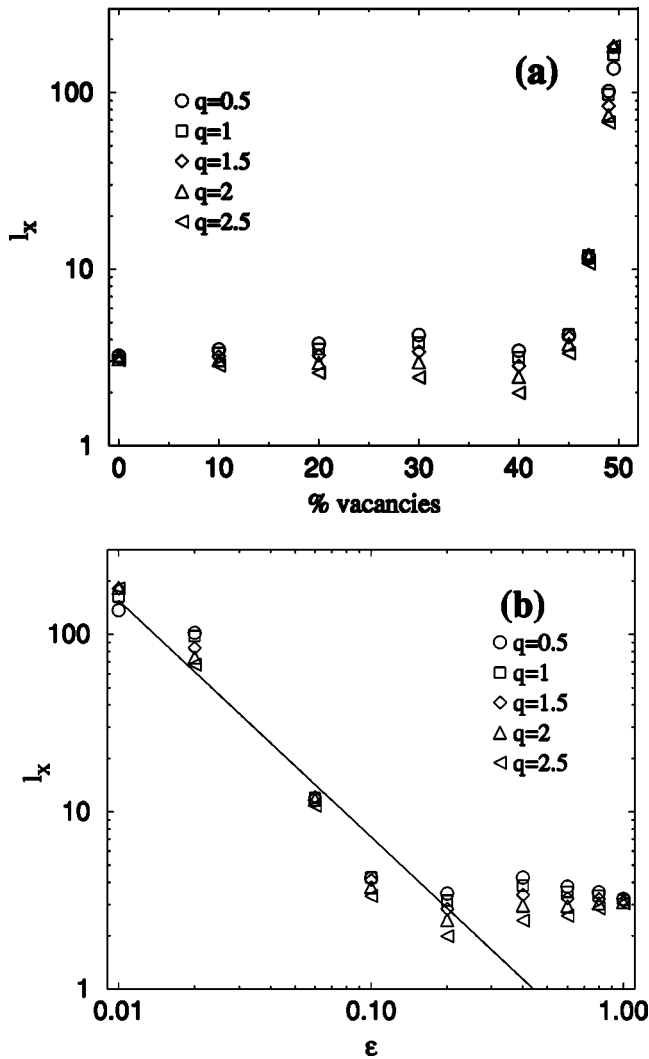In this paper we have proposed and studied a simple frustrated spring-network model which, with a relatively modest

FIG. 10. The crossover length $l_\times$ between the multiaffine regime and the saturation regime, estimated as the minimum value of L for which $H_q(L) = 0.3$. (a) Shown vs vacancy concentration on a linear-log scale. (b) Shown vs $\epsilon = 1 - (\% \text{ vacancies})/50\%$ on a log-log scale. (Note that the vacancy concentration here increases toward the *left*.) The straight line is proportional to $\epsilon^{-4/3}$, corresponding to the connectivity length for bulk site percolation [30,31]. In both parts the error bars are smaller than the symbol size.

computational effort, reproduces aspects of the scaling behavior of the surfaces of surfactant-templated polyacrylamide gels, recently observed in AFM experiments [10]. While our model does not include excluded-volume effects, which are especially important for the short-range structure of real gel systems, our results suggest that simple models that incorporate elastic properties of the gel can provide a useful framework for understanding large-scale structural characteristics of these materials, which are otherwise extremely difficult to simulate due to their complexity.

The main similarities and differences between the surface structures of our statistical-mechanical model and the experimental system by which it was inspired are as follows. *The main similarity* is a nontrivial scaling behavior corresponding to a power-law form of the increment correlation func-

tion at small and intermediate length scales. This power-law behavior terminates at a crossover length scale, above which the rms surface width and the increment correlation functions both reach saturation values that appear to be independent of the system size. The origin of this crossover behavior is explained in terms of the structural inhomogeneities of the gel. On large length scales the scaling behavior reflects the average network structure, while on small length scales the microscopic density fluctuations of the gel network play the most important role. The quantitative dependence of the crossover on the bulk vacancy concentration is discussed further below. *The main difference* between the model and the experimental surfaces lies in the details of the scaling behavior at length scales below the crossover length: the model surfaces are multiaffine, while the experimental surfaces are self-affine. The multiaffinity in the model is caused by the finite density of vertical discontinuities in the simulated surfaces (see Fig. 1), which are not seen in the experimental system (see Fig. 7 of Ref. [10]). The discontinuities in the simulated surfaces as they are defined here result from overhangs in the spring configuration at the surface, and modification of the model to improve the detailed agreement with the scaling behavior of the experimental system should aim at eliminating these overhangs. (It is also possible that overhangs do in fact exist in the undisturbed experimental surfaces, but are so mechanically weak that they are smoothed out by the force of the AFM tip.) In the model, the number and size of overhangs could be reduced or eliminated in several ways. One possibility is to simulate the smoothing action of the AFM tip, e.g., by a running-average method. Another possibility is to include a weak gravitational field (the specific gravity of the polymers is greater than that of water), which would bend overhanging sections down into the main part of the interface. It should also be noted that the larger coordination number in three dimensions most likely would reduce the importance of overhangs in a three-dimensional version of the model, even without further modifications. (Extension to three dimensions would also reduce the number of disconnected pieces, which are partly responsible for the large overhangs seen in the case of high vacancy densities. However, the computational cost would be large.) A more exhaustive numerical and analytical study of the influence of discontinuities on surface scaling behavior is currently underway [33].

The experimental surfactant templating was simulated by introducing a nonzero volume fraction of voids in the network through deleting lattice nodes and their associated springs. Both the horizontal crossover length and the vertical surface thickness (as measured by the saturation values of both the rms surface width and the generalized increment correlation functions) increase dramatically as the vacancy concentration approaches the site-percolation limit of 50%. An analogous increase of the characteristic horizontal and vertical length scales with surfactant concentration is observed in the experimental system, where it coincides with a dramatic increase in the optical opacity. The numerical results for our model thus support the hypothesis that this increase in the experimental system is caused by a percolation transition of the voids created by removal of the surfactants.

In conclusion, despite the differences in the details of the scaling behavior at small and intermediate length scales, our simplified random-spring model successfully mimics several of the surface characteristics of an important new class of porous media, including the dramatic increase in surface roughness that occurs with increasing surfactant concentration. Efforts to further improve the agreement between the small-scale scaling behavior of our theoretical model and that of the experimental system by which it was inspired are left for future study. These efforts should, in particular, involve the introduction of excluded-volume interactions and include investigations of the dependence of the scaling properties of the model on external forces due to gravity or the AFM tip, as well as on the statistics of the local spring distribution and the dimensionality of the model.

---

[1] M. Chiari and P.G. Righetti, Electrophoresis **16**, 1815 (1995).

[2] Y. Cohen, O. Ramon, I.J. Kopelman, and S. Mizrahi, J. Polym. Sci., Part B: Polym. Phys. **30**, 1055 (1992).

[3] V.G. Oshmian and L. Benguigui, J. Phys. II **6**, 1585 (1996).

[4] S. Panyukov and Y. Rabin, Macromolecules **29**, 7960 (1996).

[5] M. Shibayama, Macromol. Chem. Phys. **199**, 30 (1998).

[6] L. Benguigui and F. Boué, Eur. Phys. J. B **11**, 439 (1999).

[7] A. Suzuki, M. Yamazaki, and Y. Kobiki, J. Chem. Phys. **104**, 1751 (1995).

[8] A. Suzuki, M. Yamazaki, Y. Kobiki, and H. Suzuki, Macromolecules **30**, 2350 (1997).

[9] R.L. Rill, B.R. Locke, Y. Liu, J. Dharia, and D.H. Van Winkle, Electrophoresis **17**, 1304 (1996).

[10] M. Chakrapani, S.J. Mitchell, D.H. Van Winkle, and P.A. Rikvold, e-print cond-mat/0112255.

[11] Y. Liu and R. Pandey, J. Phys. II **4**, 865 (1994); R. Pandey and Y. Liu, J. Sol-Gel Sci. Technol. **15**, 147 (1999).

[12] G. M. Buendía, S. J. Mitchell, and P. A. Rikvold, in *Computer Simulation Studies in Condensed Matter Physics XIV*, edited by D. P. Landau, S. P. Lewis, and H.-B. Schüttler (Springer, Berlin, 2002), p. 265.

[13] E.G. Richards and C.J. Temple, Nature (London), Phys. Sci. **230**, 92 (1971).

[14] P. G. deGennes, *Scaling Concepts in Polymer Physics* (Cornell University Press, Ithaca, 1979).

[15] D.C. Liu and J. Nocedal, Math. Program. **45**, 503 (1989).

[16] The FORTRAN 77 subroutine LBFGS, equivalent to the Harwell Subroutine Library subroutine VA15, was provided by I. M. Navon.

[17] T. Vicsek, *Fractal Growth Phenomena* (World Scientific, Singapore, 1988); F. Family and T. Vicsek, *Dynamics of Fractal Surfaces* (World Scientific, Singapore, 1991).

[18] H. N. Yang, G. C. Wang, and T. M. Lu, *Diffraction from Rough Surfaces and Dynamic Growth Fronts* (World Scientific, Singapore, 1993).

[19] A. L. Barabási and H. E. Stanley, *Fractal Concepts in Surface Growth* (Cambridge University Press, Cambridge, 1995).

[20] P. Meakin, *Fractals, Scaling, and Growth far from Equilibrium* (Cambridge University Press, Cambridge, 1998).

[21] A.L. Barabási, P. Szépfalusy, and T. Vicsek, Physica A **178**, 17 (1991).

[22] A.L. Barabási and T. Vicsek, Phys. Rev. A **44**, 2730 (1991).

[23] A.L. Barabási, R. Bourbonnais, M. Jensen, J. Kertész, T. Vicsek, and Y.C. Zhang, Phys. Rev. A **45**, R6951 (1992).

[24] S. Das Sarma, C.J. Lanczycki, R. Kotlyar, and S.V. Ghaisas, Phys. Rev. E **53**, 359 (1996).

[25] C.V. Dharmadhikari, R.B. Kshirsagar, and S.V. Ghaisas, Europhys. Lett. **45**, 215 (1999).

[26] K. Kim and Y.S. Kong, J. Korean Phys. Soc. **36**, 245 (2000).

[27] K. Ivanova and M. Ausloos, Eur. Phys. J. B **8**, 665 (1999).

[28] H. Katsuragi, Physica A **278**, 275 (2000).

[29] J. Hoshen and R. Kopelman, Phys. Rev. B **14**, 3249 (1976).

[30] D. Stauffer and A. Aharony, *Introduction to Percolation Theory* (Taylor & Francis, London, 1991).

[31] S. Smirnov and W. Werner, Math. Res. Lett. **8**, 729 (2001), and references therein.

[32] R. Voss, in *Fundamental Algorithms in Computer Graphics*, edited by R. Earnshaw (Springer, Berlin, 1985).

[33] S. J. Mitchell (unpublished).